ACS APPLIED MATERIALS & INTERFACES

www.acsami.org Research Article

Self-Sensitized and Reversible O_2 Reactivity with Bisphenalenyls for Simple, Tunable, and Multicycle Colorimetric Oxygen-Sensing Films

Muhammad Imran and Mark S. Chen*

Cite This: *ACS Appl. Mater. Interfaces* 2022, 14, 1817−1825 Read Online

ACCESS | Metrics & More | Article Recommendations | Supporting Information

ABSTRACT: Monitoring the levels of molecular oxygen (O_2) is critical for numerous applications, but there is still a long-standing challenge to develop robust and cost-effective colorimetric sensors that enable detection by changes in color. Current technologies employ chromophores that require additional additives, which inherently increase the cost and complexity. Here, we report that bisphenalenyls (PQPLs) function as the single active component for colorimetric O_2 sensing through their quantitative conversion into aromatic endoperoxides (EPOs). PQPLs display self-sensitizing reactivity: they are capable of generating singlet oxygen and binding it without the need for external photosensitizers. The rates of PQPL photooxygenation depend on the electron-donating ability of substituents, which highlights a simple strategy for tuning O_2 sensitivity. EPOs are stable under ambient conditions but can be thermally stimulated to convert back to PQPLs and concomitantly release O_2. Polymer-supported (PTMSP) films of PQPLs (2 wt %) reproduce these reactivity trends with a rapid red-to-colorless transition that is visible to the naked eye within 1 h of exposure and show a very low limit of detection (<5 ppm O_2). Films are chemically and thermally robust and maintain up to >99% of their original colorimetric response when reused and subjected to multiple cycles of photooxygenation and O_2 release. The simplicity and solution processability of these materials highlight their potential as "intelligent" inks for printable colorimetric sensors.

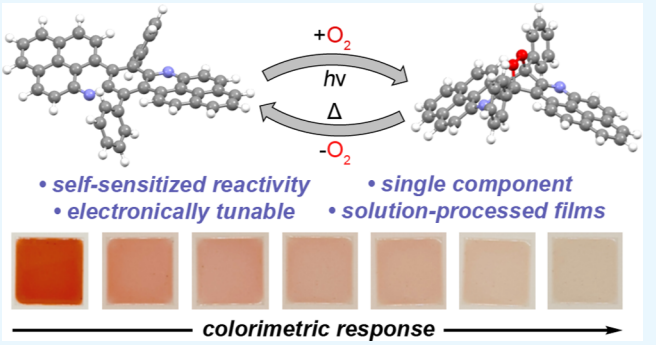

KEYWORDS: *singlet oxygen, self-sensitization, photosensitizer, aromatic endoperoxide, photochromic, colorimetric*

INTRODUCTION

Technologies for monitoring molecular oxygen (O_2) levels are important for safety and minimizing waste since many materials are susceptible to oxidative degradation through processes such as metal corrosion and food spoilage.[1,2] Electrochemical assays are the most common method for monitoring dissolved O_2 levels, while fluorometric measurements have emerged as the predominant method for monitoring gaseous O_2.[3] Luminescence-based methods are fast, accurate, and tunable to a wide range of sensitivities; however, they often rely on expensive precious metals as emissive materials. Additionally, luminescence analysis requires the skilled operation of a spectrofluorometer, which further diminishes the suitability of luminescent sensors for applications limited by cost, complexity, and toxicity.[4,5]

To avoid the need for analytical instrumentation, monitoring O_2 levels can alternatively be accomplished with colorimetric (color-based) sensors. Since these systems undergo a change in color hue or intensity upon oxidation, they can be monitored by simple optical detection methods such as the naked eye. Colorimetric systems have been reported in the literature, and a few are commercially available.[6−16] However, these sensors still find limited use because they are often complex mixtures that consist of a redox dye, a sacrificial reductant, and a photocatalyst or a base, which leads to increased costs and difficulties in handling and storage (Figure 1a). To mitigate such complications, an O_2 sensor that relies on fewer, possibly even just one, metal-free materials would be advantageous. With fewer components, such a sensor would be well-suited for applications such as modified atmosphere packaging, where indicators need to be inexpensive (i.e., printable) and simple to measure (i.e., visible to the human eye).[17,18]

Among materials for sensing, aromatic compounds are attractive for their tunable chemical and luminescence properties.[19−21] Acenes in particular have been well-studied for O_2 sensing as they are known to bind O_2 to generate aromatic endoperoxides (EPOs) via formal [4 + 2] cycloaddition (Figure 1b).[22−31] Conversion of aromatic acenes into EPOs promotes changes in fluorescence that enable highly

Received: August 22, 2021
Accepted: December 13, 2021
Published: December 27, 2021

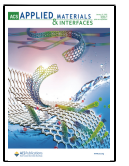

https://doi.org/10.1021/acsami.1c16033
ACS Appl. Mater. Interfaces 2022, 14, 1817−1825

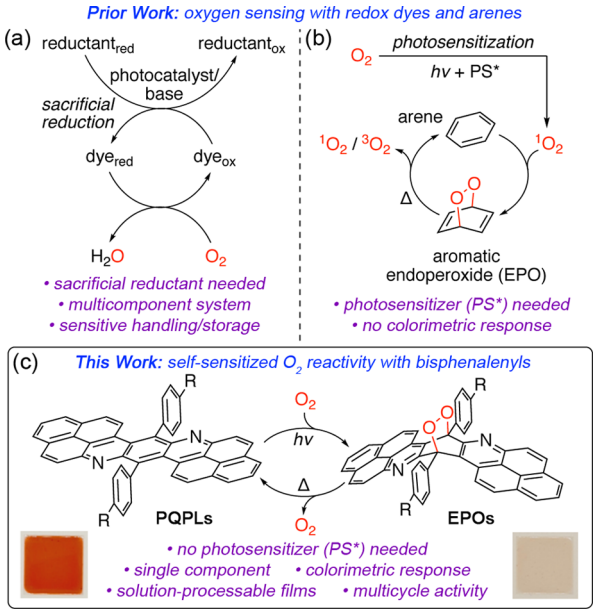

Figure 1. Prior strategies for oxygen-sensing with (a) redox dyes and (b) arenes that react with O_2 to form aromatic EPOs. (c) Self-sensitizing PQPLs reported in this study that enable the solution-processing of single-component colorimetric films that change from red (PQPL) to colorless (EPO) upon binding O_2.

accurate, ratiometric O_2 measurements.[32−34] EPOs are often persistent at room temperature but can undergo cycloreversion upon heating to release O_2 and regenerate the parent acene.[35−37] Due to this reversible reactivity, acene-based materials have also been investigated for oxygen storage, molecular switches, and photodynamic therapy.[38−42]

Despite their common use as fluorescent materials, acenes are yet to be employed as sensors by exploiting O_2-promoted color changes.[43] Most studies have focused on shorter, easier-to-synthesize compounds (i.e., naphthyl and anthracenyl) that are colorless in both their aromatic and oxidized forms. Colored acenes that react with O_2 are certainly precedented but are yet to explicitly demonstrate colorimetric sensing applications.[44,45] Additionally, nearly all reports of EPO formations require an external photosensitizer (PS*) to convert triplet oxygen ($^3O_2$) into its metastable singlet state ($^1O_2$) since $^3O_2$ is often insufficient for reactivity.[46−51] Therefore, for a single molecule to meet all the requirements for a simple, colorimetric O_2 sensing material, it must react with O_2 to induce a visible color change and demonstrate self-sensitizing O_2 reactivity.

In this work, we have discovered colorimetric O_2-sensing films that employ a series of PQPL (pyridoquinoline diphenalene) molecules capable of self-sensitizing reactivity with O_2 that transform from red PQPLs (**1**−**3**) into colorless EPOs (**1-O$_2$**, **2-O$_2$**, and **3-O$_2$**) (Figure 1c). Photooxygenations proceed quantitatively in the absence of external photosensitizers, and higher reaction rates correlate with the increasing electron-rich substitution. Colorless EPOs are very stable under ambient conditions but can be stimulated to release O_2 upon heating (thermolysis). Solution-processed PQPL/PTMSP (2 wt %) blend films show a very low limit of detection (<5 ppm O_2) that enables them to display a colorimetric response to visible light and O_2 within minutes of exposure. The robust films maintain a high response through multiple O_2 binding and release cycles and demonstrate that PQPLs can serve as the single active component in reusable, solution-processed, and colorimetric O_2-sensing films.

RESULTS AND DISCUSSION

Synthesis and Characterization of Optical and Electrochemical Properties. Target PQPLs (**1**−**3**) with varying electronic substitution were constructed by adapting synthetic procedures from our previous bisphenalenyl synthetic studies.[52,53] Suzuki−Miyaura cross-coupling with commercially available phenylboronic acids enabled rapid access to varied dibromoterphenyl precursors (Scheme 1). The dibromoterphenyls were then coupled to 2 equivalents of phenalenone to provide PQPLs **1**−**3** after the completion of a five-step reaction sequence.

Scheme 1. Synthesis of PQPLs (1−3) from Commercial Boronic Acids via Coupling with Phenalenone

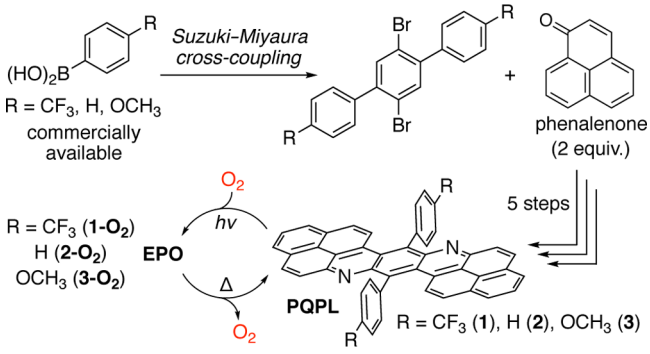

Corresponding to their red color, each PQPL demonstrates strong UV absorption ($\lambda_{max} \approx 355$ nm) and several weaker, visible bands between 440 and 590 nm (Figures 2a, S1). We observed that solutions of **1**-**3** would bleach to colorless when left exposed to air and light overnight, so we analyzed the solutions by nuclear magnetic resonance (NMR) and

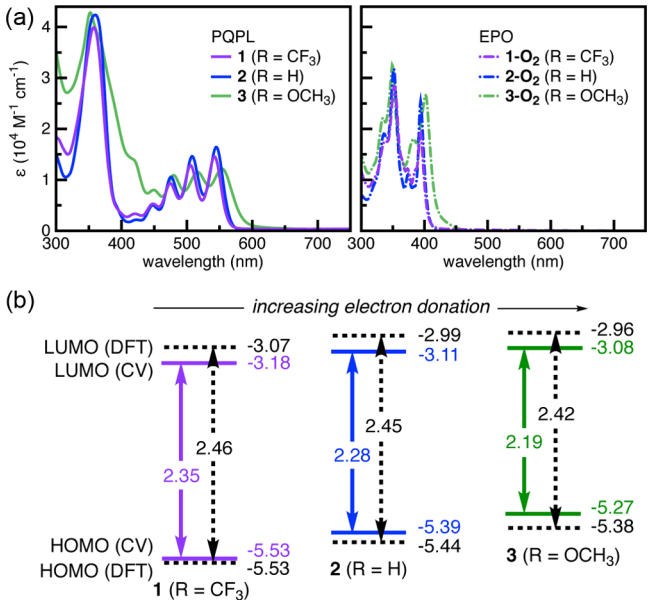

Figure 2. (a) Absorption spectra of PQPLs (left, solid) and EPOs (right, dashed). (b) HOMO and LUMO energy levels determined by cyclic voltammetry (solid) and density functional theory (dotted).

https://doi.org/10.1021/acsami.1c16033
ACS Appl. Mater. Interfaces 2022, 14, 1817−1825

determined that the color loss resulted from the formation of EPOs (**1-O$_2$**, **2-O$_2$**, and **3-O$_2$**). Absorption spectroscopy confirmed that none of the EPOs absorb wavelengths >450 nm (Figures 2a, S2), which supports the visible color change that accompanies the transformation of red PQPLs into colorless EPOs.

Electrochemical characterization using cyclic voltammetry and simulation using the density functional theory both reveal a direct relationship between electronic substitution and molecular orbital energy levels (Figures 2b, S3, and S4). Higher HOMO (highest occupied molecular orbital) and LUMO (lowest unoccupied molecular orbital) energy levels correlate with the presence of electron-rich (**3**) versus electron-poor (**1**) functional groups. Given that the EPO formation proceeds through the oxidation of PQPLs, higher HOMO energy levels are expected to cause higher rates of reactivity and a faster color change. If the reactivity rates of PQPLs can be tailored via synthetic modification, then it is likely that materials can be engineered with varying degrees of colorimetric sensitivity and can therefore be employed in a wider variety of applications.

Photoluminescence and Singlet Oxygen Sensitization. Each PQPL (**1**−**3**) is photoluminescent (λ_{ex} = 500 nm) with emissions in the visible and near-infrared (NIR) regions, all of which are significantly redshifted from the photoluminescence (λ_{ex} = 370 nm) emissions of their corresponding EPOs (Figures 3a and S8−S10 and Table 1). These large

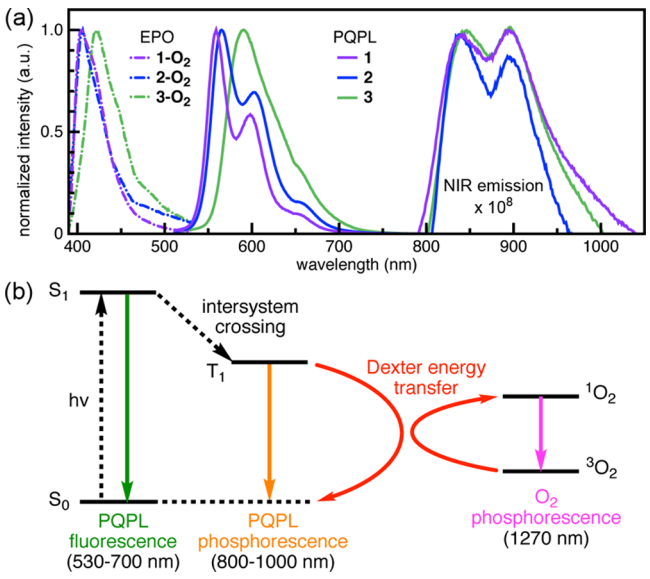

Figure 3. (a) Photoluminescence spectra of PQPL (solid) and EPOs (dashed) in the visible and NIR regions. (b) Proposed Jablonski diagram that relates the photophysical properties and excited states of PQPL and the observation of $^1O_2$ sensitization.

Table 1. Photoluminescence and Reactivity Rates of PQPLs

PQPL	λ_{Fl} [nm][a]	τ_{Fl} [ns]	Φ_{Fl}	λ_{Ph} [nm][a]	$t^{1/2}$ [min]	10^{-4} k [s^{-1}]
1	559, 598	2.29	0.87	837, 896	35.0 ± 3.2	3.30 ± 0.3
2	565, 603	2.76	0.85	841, 895	30.1 ± 0.9	3.80 ± 0.1
3	590	2.42	0.63	841, 896	11.3 ± 1.1	9.99 ± 1.0

[a]Excitation (λ_{ex}) at 500 nm.

spectral shifts suggest that O_2 sensing might be performed by monitoring changes in the emission spectra; however, our studies focused on colorimetric sensing for its simplicity and easy readout when compared to that of fluorometric methods. Nevertheless, the characterization of these emissive excited states was extremely helpful for understanding the photophysical properties of PQPLs.

The visible emission of **1**−**3** (540−700 nm) displays a relatively high quantum yield (63−87%) and a short luminescence lifetime (<3 ns) (Figures S11 and S13). In combination with TDDFT/B3LYP-calculated electronic transitions, these data suggest that the orange emission corresponds to fluorescence via the radiative decay (LUMO → HOMO) from an excited singlet (S_1) (Tables S13−S15). The broad NIR emission (800−950 nm) is observed in oxygen-free solutions of **1**−**3** and, due to its correspondence with a lower energy transition, likely represents phosphorescence via the radiative decay from an excited triplet (T_1) (Figures S14 and S15). TDDFT/UB3LYP calculations slightly underestimate the energy for this NIR transition but still support that it results from the radiative decay (LUMO → HOMO) from T_1 to S_0 (Tables S16−S18).

When solutions of **1**−**3** are saturated with O_2, the NIR emission is conspicuously absent, and instead, a longer wavelength emission (λ_{max} = 1270 nm) diagnostic for the radiative decay of singlet oxygen ($^1O_2$) is observed (Figure S16).[54] These spectroscopic behaviors are reminiscent of other known photosensitizers (i.e., rose bengal and methylene blue) and suggest that **1**−**3** possess an emissive triplet excited state (T_1) that is energetically accessible upon photoexcitation and capable of sensitizing singlet oxygen. PQPLs **1**, **2**, and **3** display similar $^1O_2$ quantum yields of 11, 9, and 11%, respectively (Figures S17−S19).[55−57]

These spectroscopic data allow us to infer several relationships between the photophysical processes observed with PQPLs (Figure 3b). Photoexcitation generates an excited singlet (S_1) that can either radiatively decay (visible fluorescence) back to S_0 or undergo intersystem crossing to generate an excited triplet (T_1). When O_2 is absent, relaxation of T_1 is observed by NIR emission (phosphorescence). However, when O_2 is present, T_1 is capable of undergoing a Dexter energy transfer to sensitize singlet oxygen ($^1O_2$), which we observe when it radiatively decays (λ_{max} = 1270 nm) to its triplet ground state ($^3O_2$). Since no other photoactive compound is present, we can infer that PQPLs **1**−**3** are sufficient photosensitizers of O_2. Moreover, due to this self-sensitizing reactivity of PQPLs, it is strongly suggested that $^1O_2$ is the active oxidant in the formation of EPOs.

Electronic Effects on Photooxygenation Rates. Solutions of **1**−**3** exposed to ambient air and light diminish in color intensity over time and show different EPO formation rates based on electronic substitution (Figures 4a and S20). Kinetic studies of the photooxygenation of PQPLs **1**−**3** were performed by exposing O_2-saturated dichloromethane solutions of **1**−**3** to a green light-emitting diode (LED) (530−550 nm) and ambient white light irradiation at room temperature, and monitoring them using UV−visible spectroscopy over 24 h (Figures 4b−e and S22). Photooxygenation rates (k) of **1**−**3** were calculated according to pseudo-first-order kinetics by plotting $\ln(A/A_0)$ *versus* time (Figure S21). Similar to previous reports of EPO formations, rates of photooxygenation correlate with HOMO energy levels, where the most electron-rich PQPL (**3**) demonstrates the highest

https://doi.org/10.1021/acsami.1c16033
ACS Appl. Mater. Interfaces 2022, 14, 1817−1825

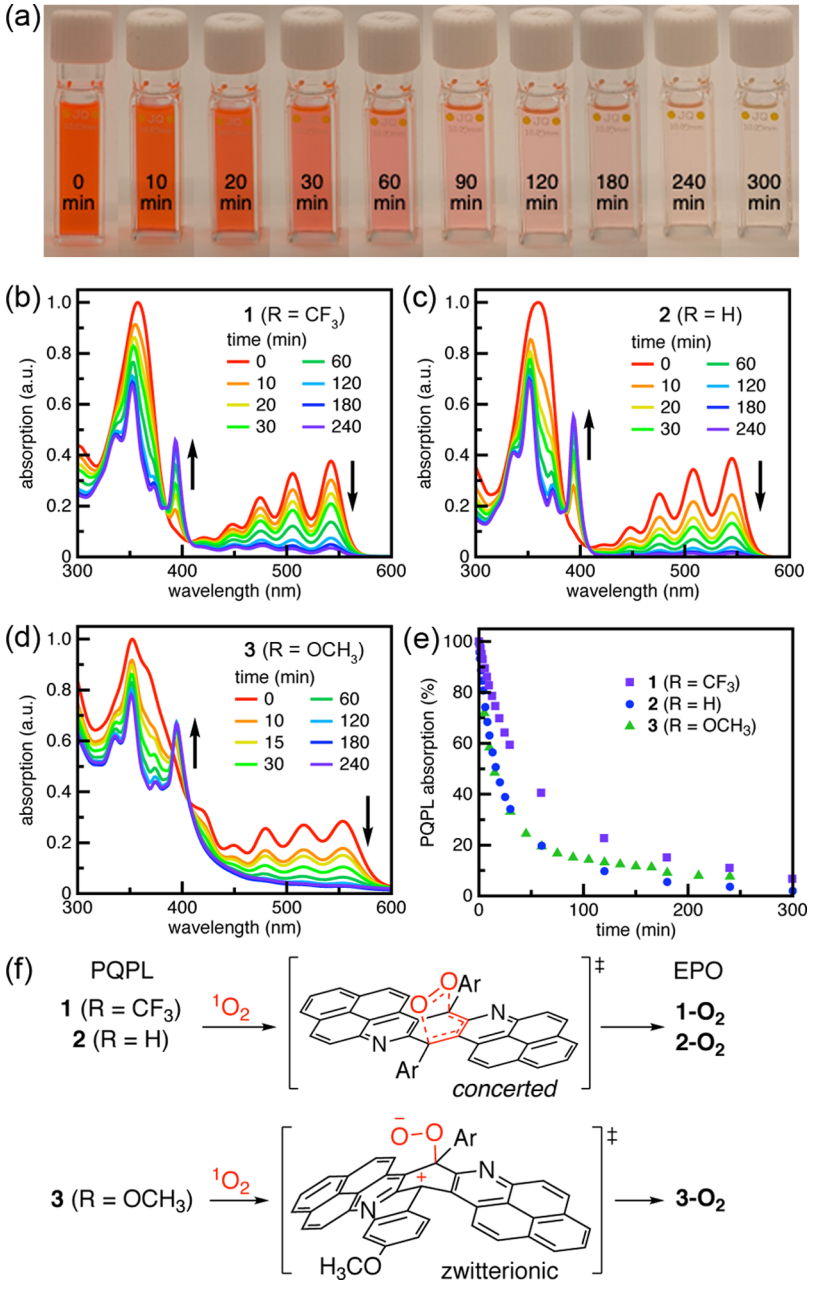

Figure 4. (a) Photographs of **2** at various time intervals upon exposure to ambient air and light. Plots depicting the change in the absorption spectra of **1** (b), **2** (c), and **3** (d) during the first 4 h of self-sensitized oxygenation. (e) Plot of absorption decrease vs time of the longest wavelength absorption peak in **1**–**3** due to photooxygenation. (f) Proposed transition states for PQPL photooxygenations.

reaction rate and the most electron-poor PQPL (**1**) demonstrates the lowest (Table 1).[58] This trend is also observed when photooxygenations are performed under red LED (630–700 nm) irradiation in the presence of methylene blue so that $^1O_2$ is exclusively generated by the external photosensitizer (Figure S24 and Table S8).

To correlate the relative photooxygenation rates with electronic substituent effects, we performed Hammett analysis on our kinetic data. Photooxygenations with methylene blue show a linear free energy relationship with a smaller negative reaction constant ($\rho = -0.483$) than that in previous reports of EPO generation.[58−60] This correlation argues against a charged transition state for one that is less sensitive to electronic effects, such as a concerted process (Figure S25).

In contrast, when PQPL is relied upon for photosensitization, the substituent effects on the reaction rate display a nonlinear trend where rates for **1** and **3** are lower and higher than expected, respectively (Figure S23). This deviation suggests that electron-donating groups alter the mechanism from a concerted process since $\rho = 1.5664$ when $\sigma_p < 0$ (electron-rich), which is more negative than $\rho = -0.483$ obtained using an external photosensitizer and $\rho = -0.1135$ when $\sigma_p > 0$ (electron-poor). We postulate that an electron-donating group enhances the photooxygenation rate of **3** by stabilizing a zwitterionic superoxide transition state (Figure 4f). Although specific mechanisms may vary, these data clearly demonstrate that PQPL photooxygenation rates are tunable and should enable the tailoring of the materials' O_2 response.

https://doi.org/10.1021/acsami.1c16033
ACS Appl. Mater. Interfaces 2022, 14, 1817−1825

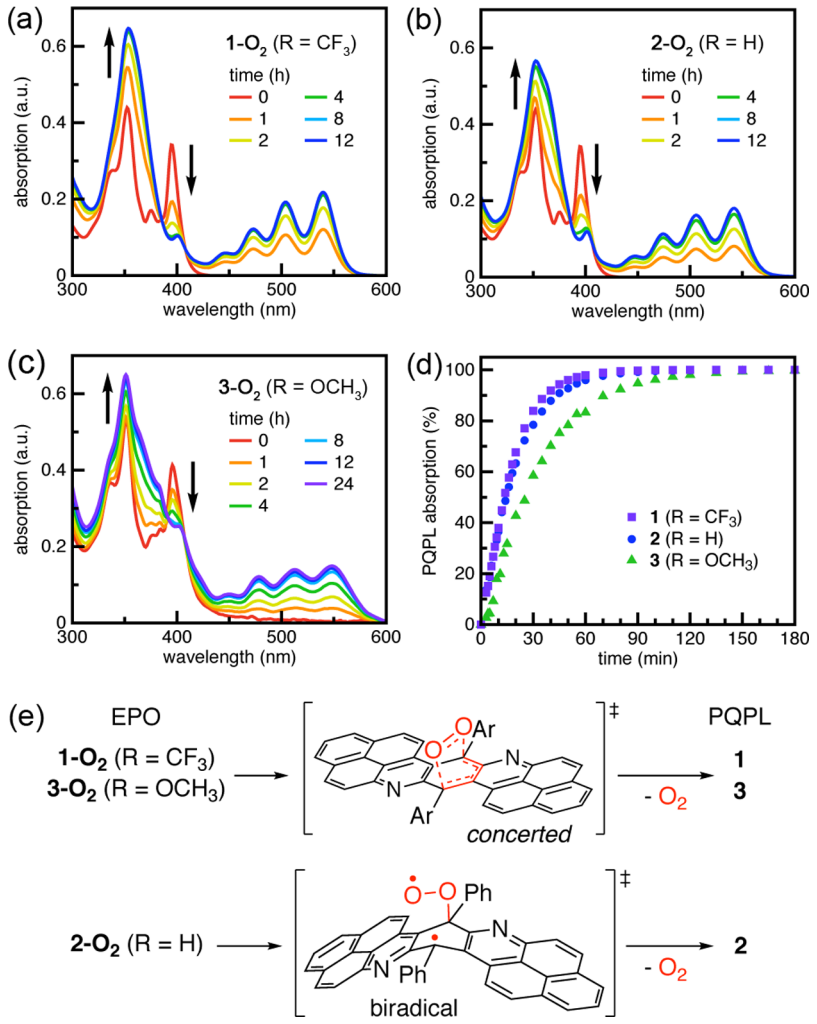

Figure 5. Plots depicting the change in absorption spectra of **1-O$_2$** (a), **2-O$_2$** (b), and **3-O$_2$** (c) during the first 12−24 h of thermolysis at 100 °C. (d) Plot of absorption change vs time due to EPO thermolysis, monitored by measuring the growth of the longest wavelength absorption peak in **1**−**3**. (e) Proposed transition states for EPO thermolysis.

Table 2. Kinetic and Thermodynamic Parameters for Cycloreversion of EPOs (1-O$_2$, 2-O$_2$, and 3-O$_2$)

EPO	$t^{1/2}$ [s][a]	10^{-4} k [s^{-1}][a]	ΔE_a [kJ mol^{-1}]	ln A	$\Delta H^{\ddagger}$ [kJ mol^{-1}]	$\Delta S^{\ddagger}$ [J K^{-1} mol^{-1}]
1-O$_2$	459 ± 155	11.3 ± 1.3	112 ± 3	29.4 ± 1	109 ± 3	−10.8 ± 8
2-O$_2$	705 ± 34	8.96 ± 0.2	124 ± 3	33.1 ± 1	121 ± 3	20.3 ± 8
3-O$_2$	1086 ± 127	5.44 ± 0.4	105 ± 2	26.9 ± 0.6	102 ± 2	−31.5 ± 5

[a]Measured at 373 K in chlorobenzene.

Oxygen Release Activated by Heat. The EPOs generated through photooxygenation are very stable at room temperature but can be stimulated to release O$_2$ at higher temperatures (thermolysis). In this process, each EPO (**1-O$_2$**, **2-O$_2$**, and **3-O$_2$**) quantitatively converts back to its respective parent arene (**1**−**3**) (Figure 5a−d). Cycloreversion rates follow first-order kinetics, where half-life ($t^{1/2}$) values at 100 °C are calculated to range between 459 and 1086 s (Table 2 and Figure S26). The release of O$_2$ shows a reactivity trend inverse to that of photooxygenation, where the fastest rate is obtained with the least electron-rich EPO (**3-O$_2$**). Electronic substituent effects show a linear free energy relationship in a Yukawa−Tsuno versus Hammett plot and indicate that resonance effects cause a negative deviation in the relative thermolysis rate of **3-O$_2$** (Figure S27). However, since a zwitterionic mechanism with a negative charge buildup is inconsistent with the small positive reaction constant (ρ = 0.2255), we infer that the resonance effects in **3-O$_2$** likely result from ground-state stabilization via π-donation into an antibonding orbital (σ^* C−O) of the endoperoxide moiety.

Arrhenius and Eyring analyses of kinetic data collected at different temperatures (80−100 °C) enable the determination of thermodynamic parameters for O$_2$ release (Figures S28−S33). **2-O$_2$** displays relatively higher activation energies (ΔE_a) and enthalpies ($\Delta H^{\ddagger}$) than **1-O$_2$** or **3-O$_2$**. Additionally, the activation entropy ($\Delta S^{\ddagger}$) for **2-O$_2$** is positive and contrasts with $\Delta S^{\ddagger} < 0$ for **1-O$_2$** and **3-O$_2$**. These disparities suggest that the thermolysis of **2-O$_2$** proceeds via a stepwise biradical mechanism, while **1-O$_2$** and **3-O$_2$** undergo a concerted process (Figure 5e).[61,62] We postulate that this mechanistic divergence is caused by polarization in electronically biased (**1-O$_2$** and **3-O$_2$**) versus unsubstituted (**2-O$_2$**) EPOs. The negative $\Delta S^{\ddagger}$ in

https://doi.org/10.1021/acsami.1c16033
ACS Appl. Mater. Interfaces 2022, 14, 1817−1825

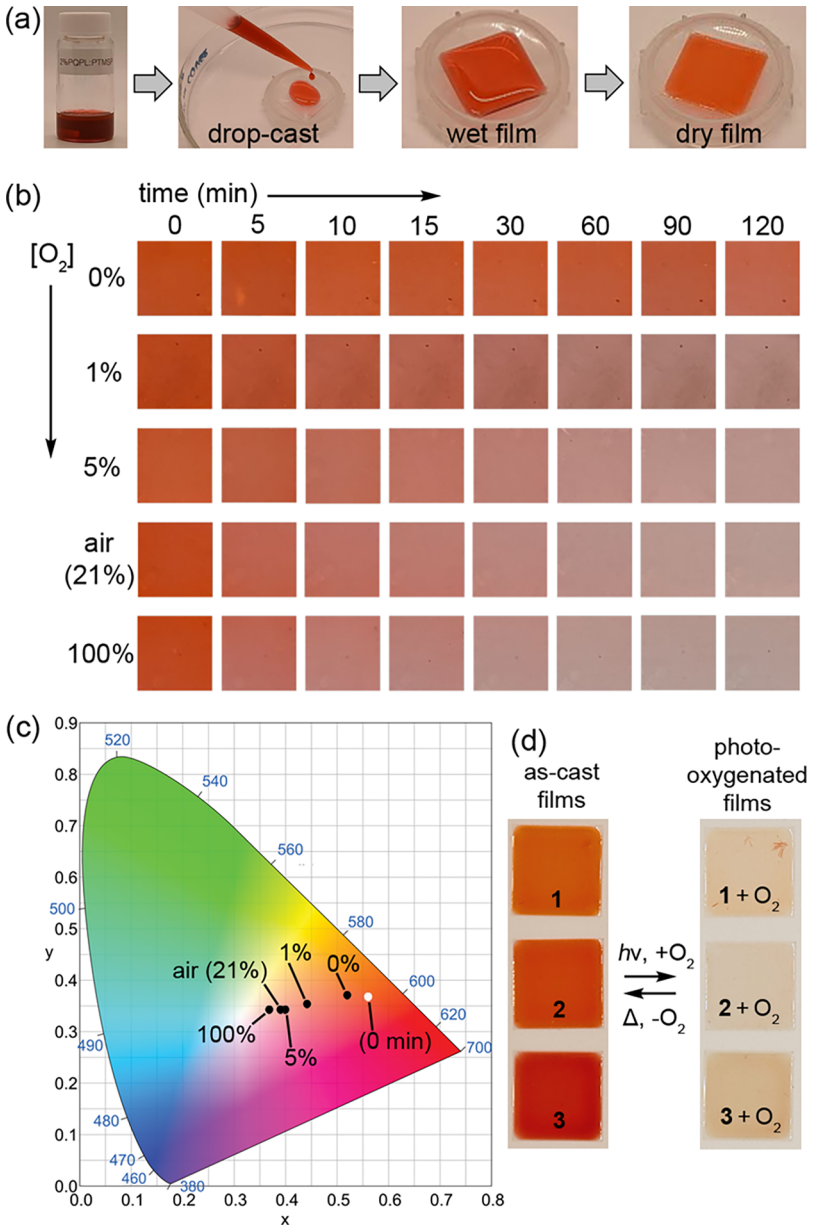

Figure 6. (a) Photographs demonstrating the drop-casting process for generating 2 wt % PQPL/PTMSP films. (b) Photographs of **2**:PTMSP films during the first 2 h of exposure to light in atmospheres with varying O_2 concentrations. (c) Chromaticity coordinates (CIE 1931) of **2**:PTMSP films in varying O_2 concentrations after 30 min. (d) Photographs of PQPL/PTMSP films that depict the color difference between the as-cast (red) and photooxygenated (colorless) films.

1-O$_2$ and **3-O$_2$** likely results from the concerted transition state requiring the coplanarization of the bent π-backbone, which is induced by significant steric congestion. Therefore, of the three EPOs, only **1-O$_2$** fulfills the principle of microscopic reversibility, where the photooxygenation and thermolysis proceed through the same, concerted transition state.

Oxygen Sensing in Polymer-Supported Colorimetric PQPL Films. Having clarified the interconversion mechanisms between red PQPLs (**1**−**3**) and their respective colorless EPOs (**1-O$_2$**, **2-O$_2$**, and **3-O$_2$**), we sought to evaluate how these properties apply in the solid state. Films were obtained by drop-casting from chlorobenzene solutions of PQPL/PTMSP (2 wt %) on glass slides (Figure 6a). PTMSP (poly[1-(trimethylsilyl)-1-propyne]) was chosen as the polymer support due to its high oxygen permeability and its solubility in a wide range of organic solvents. The PQPL/PTMSP films demonstrate similar absorption and emission properties, albeit slightly blue-shifted (~7 nm) as compared to that of PQPL solutions (Figures S35 and S36). Films generated in this manner demonstrate a uniform thicknesses of 21−24 μm (Table S9) and thermal stabilities up to 300 °C (Figures S37 and S38).

Upon exposure to light and ambient air, the films' red color intensity diminishes until they appear colorless within a few hours (Figures 6b). The absorption spectra of bleached films are identical to those of EPO in solution, which suggests that dispersed PQPLs undergo photooxygenation with O_2 that is absorbed by the polymer films. Reactivity rates follow pseudo-first-order kinetics and correspond to a half-life ($t^{1/2}$) between 1 and 14 min for PQPL/PTMSP films (Figure S39, Table S10). These data confirm that solid-state and solution

https://doi.org/10.1021/acsami.1c16033
ACS Appl. Mater. Interfaces 2022, 14, 1817−1825

reactivity trends are similar: photooxygenation rates are higher in **3**:PTMSP and lower in **1**:PTMSP.

Since O_2 is critical for photooxygenation, we sought to examine the effects of O_2 concentration ($[O_2]$) on the colorimetric response. By exposing **2**:PTMSP films to atmospheres of varying mixtures of O_2 and N_2, we observed that higher $[O_2]$ correlated with faster film bleaching (Figures 6b and S41). By plotting the chromaticity coordinates of the various films in the CIE 1931 color space, we observe that photooxygenation correlates with a decrease in the CIE x-coordinate (Figures 6c and S42). The red color even diminishes under very low $[O_2]$ conditions (<5 ppm O_2), which indicates that these films have a very low limit of detection (Figure S43). Determination of specific $[O_2]$ would be difficult from these films; however, such a measurement is often not the purpose of colorimetric sensors. Colorimetric versus fluorescence O_2 sensing is advantageous when one requires the indication of exposure relative to a defined threshold (i.e., food spoilage) rather than precise quantitative measurement. The array of photographs show that PQPL/PTMSP films are capable of such detection since higher $[O_2]$ merely enhances the rate of photooxygenation. We posit that the normalization of processing conditions and the use of calibrated color standards will enable O_2 detection that is simple and instrument-free, akin to a pH indicator paper.

Since reusability is advantageous for lowering material costs, we investigated the reversibility of these films over multiple cycles of O_2 binding and release by UV−visible spectroscopy (Figure 6d). Each PQPL/PTMSP film was subjected to at least five cycles of photooxygenation and thermolysis (150 °C) for 2 h while measuring the intensity of the longest wavelength absorption. The change in intensity at each successive cycle was compared to that of the initial photooxygenation to evaluate the photochromic fatigue. After five cycles, **2**:PTMSP films maintain a colorimetric response that is visible to the naked eye, but the absorption change (λ_{abs} = 542 nm) is 83% of the first photooxygenation (Figure 7a). The decline in absorption change (λ_{abs} = 535 nm) is less in **1**:PTMSP films, which show 90% of the initial colorimetric response in the fifth photooxygenation (Figure 7b). Notably, the decline in colorimetric response is negligible in **3**:PTMSP films as the fifth photooxygenation still demonstrates >99% of the initial absorption change (λ_{abs} = 544 nm) (Figure 7c). By comparison, dichlorobenzene solutions of **1**−**3** show greater declines in colorimetric response (75−80%) by the fifth photooxygenation, which indicates that the fatigue is diminished in the solid state compared to that in more disordered solutions (Figure S34). Low photochromic fatigue illustrates the chemical and thermal robustness of these films, especially since photooxygenation and thermolysis likely coincide with high concentrations of reactive $^1O_2$. Infrared spectra of **2**:PTMSP films prior to and after multiple photooxygenation cycles are identical and indicate that any oxidative degradation of the polymer support by reactive oxygen species is extremely minimal (Figures 7d, S44).

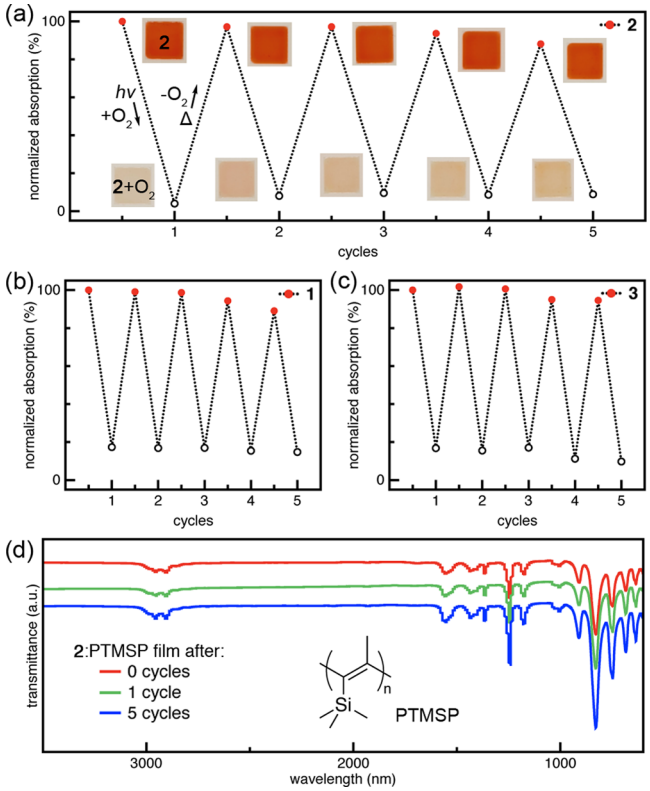

Figure 7. Plots of the longest wavelength absorption intensity vs cycle of (a) **2**:PTMSP, (b) **1**:PTMSP, and (c) **3**:PTMSP films after five cycles of photooxygenation. (d) Comparisons of infrared spectra of deoxygenated **2**:PTMSP films after various cycles of O_2 binding and release.

CONCLUSIONS

We have discovered a series of red-colored PQPLs (**1**−**3**) that display self-sensitizing reactivity toward O_2 to quantitatively transform into colorless EPOs (**1**−**3**-O_2) without the need for additional photosensitizers. Rates of PQPL (**1**−**3**) photooxygenation via O_2 binding are tunable by appending different electron-donating or -withdrawing substituents and trend with the increasing electron density on the π-backbone. Cycloreversion of EPOs (**1**−**3**-O_2) to release O_2 is promoted by heat (thermolysis), which regenerates the parent PQPLs (**1**−**3**) and alludes to the potential for these molecular materials to be recyclable. These trends and color changes also proceed in PTMSP polymer-supported films of PQPL (2 wt %) that show fast response times (minutes), low limits of detection (<5 ppm O_2), and retain nearly all colorimetric activity after multiple cycles of O_2 binding and release. The solution processability and simplicity of this organic material illustrate its potential as an "intelligent" ink for printing scalable and inexpensive colorimetric oxygen-sensing films. Additionally, the photosensitizing properties of these compounds and their tunable reactivity with oxygen bear significance for photodynamic therapy, singlet oxygen probes, and photocatalysis.

ASSOCIATED CONTENT

Supporting Information

The Supporting Information is available free of charge at https://pubs.acs.org/doi/10.1021/acsami.1c16033.

Synthetic procedures, spectroscopic methods, kinetics measurements, details of experimental methods, UV−visible absorption spectra, cyclic voltammograms, HOMO and LUMO orbital plots, optimized geometries, emission spectra, transient photoluminescence decay spectra, phosphorescence NIR emission plots, determination of $^1O_2$ quantum yields, photographs of the color change of PQPLs, logarithmic plot of the absorption change for solutions of PQPLs, plots of photo-

https://doi.org/10.1021/acsami.1c16033
ACS Appl. Mater. Interfaces 2022, 14, 1817−1825

oxygenation in DCM solutions of PQPLs, Hammett plots, Yukawa−Tsuno plots, thermolysis of **1-O$_2$**, **2-O$_2$**, and **3-O$_2$** and their corresponding Arrhenius and Erying plots, thermogravimetric analysis curves, differential scanning calorimetry thermograms, plots of photooxygenation of PQPL:PTMSP films, photographs of **2**:PTMSP films irradiated under atmospheres of varying oxygen concentrations, plots of the CIE x-coordinate versus time, absorption and Fourier transform infrared spectra, NMR spectra, and computational outputs (PDF)

AUTHOR INFORMATION

Corresponding Author

Mark S. Chen − *Department of Chemistry, Lehigh University, Bethlehem, Pennsylvania 18015-3102, United States;* orcid.org/0000-0001-5415-4660; Email: mschen@lehigh.edu

Author

Muhammad Imran − *Department of Chemistry, Lehigh University, Bethlehem, Pennsylvania 18015-3102, United States*

Complete contact information is available at: https://pubs.acs.org/10.1021/acsami.1c16033

Notes

The authors declare the following competing financial interest(s): The authors are inventors on a U.S. provisional patent filing by Lehigh University covering the herein-described synthetic process and example compounds and films.

ACKNOWLEDGMENTS

The authors thank Dr. C. M. Wehrmann, G. Y. Rojas, Prof. Lisa A. Fredin, and Prof. Elizabeth R. Young for helpful discussions. Acknowledgement is made of the Donors of the American Chemical Society Petroleum Research Fund for partial support of this research (61890-ND4). Support was also provided by a National Science Foundation CAREER award (CHE-2045920) and Lehigh University. M.I. thanks the Fulbright Program for a Predoctoral Graduate Fellowship. This work made use of the Lehigh University NMR Facility and a Bruker Neo 500 MHz NMR system that was acquired through NSF-MRI-1725883 with additional support from Lehigh University.

REFERENCES

(1) Ogilby, P. R. Singlet Oxygen: There is Indeed Something New Under the Sun. *Chem. Soc. Rev.* **2010**, *39*, 3181−3209.

(2) Greer, A. Foote's Discovery of the Role of Singlet Oxygen [$^1O_2$ ($^1\Delta_g$)] in Photosensitized Oxidation Reactions. *Acc. Chem. Res.* **2006**, *39*, 797−804.

(3) Wolfbeis, O. S. Luminescent Sensing and Imaging of Oxygen: Fierce Competition to the Clark Electrode. *Bioessays* **2015**, *37*, 921−928.

(4) Wang, X.-d.; Wolfbeis, O. S. Optical Methods for Sensing and Imaging Oxygen: Materials, Spectroscopies and Applications. *Chem. Soc. Rev.* **2014**, *43*, 3666−3761.

(5) Schäferling, M. The Art of Fluorescence Imaging with Chemical Sensors. *Angew. Chem., Int. Ed.* **2012**, *51*, 3532−3554.

(6) Son, E. J.; Lee, J. S.; Lee, M.; Vu, C. H. T.; Lee, H.; Won, K.; Park, C. B. Self-adhesive Graphene Oxide-Wrapped TiO_2 Nanoparticles for UV-Activated Colorimetric Oxygen Detection. *Sens. Actuators, B* **2015**, *213*, 322−328.

(7) Mills, A.; Lawrie, K.; Bardin, J.; Apedaile, A.; Skinner, G. A.; O'Rourke, C. An O_2 Smart Plastic Film for Packaging. *Analyst* **2012**, *137*, 106−112.

(8) Wilhelm, S.; Wolfbeis, O. S. Irreversible Sensing of Oxygen Ingress. *Sens. Actuators, B* **2011**, *153*, 199−204.

(9) Roberts, L.; Lines, R.; Reddy, S.; Hay, J. Investigation of Polyviologens as Oxygen Indicators in Food Packaging. *Sens. Actuators, B* **2011**, *152*, 63−67.

(10) Mills, A.; Lawrie, K. Novel Photocatalyst-based Colourimetric Indicator for Oxygen: Use of a Platinum Catalyst for Controlling Response Times. *Sens. Actuators, B* **2011**, *157*, 600−605.

(11) Mills, A.; Hazafy, D.; Lawrie, K. Novel Photocatalyst-based Colourimetric Indicator for Oxygen. *Catal. Today* **2011**, *161*, 59−63.

(12) Mills, A.; Hazafy, D. Nanocrystalline SnO2-based, UVB-activated, Colourimetric Oxygen Indicator. *Sens. Actuators, B* **2009**, *136*, 344−349.

(13) Mills, A.; Hazafy, D. A Solvent-based Intelligence Ink for Oxygen. *Analyst* **2008**, *133*, 213−218.

(14) Lee, S.-K.; Sheridan, M.; Mills, A. Novel UV-Activated Colorimetric Oxygen Indicator. *Chem. Mater.* **2005**, *17*, 2744−2751.

(15) Lee, S.-K.; Mills, A.; Lepre, A. An intelligence ink for oxygen. *Chem. Commun.* **2004**, 1912−1913.

(16) Lee, S.-K.; Mills, A. Novel photochemistry of leuco-Methylene Blue. *Chem. Commun.* **2003**, 2366−2367.

(17) Yousefi, H.; Su, H.-M.; Imani, S. M.; Alkhaldi, K.; Filipe, C. D.; Didar, T. F. Intelligent Food Packaging: A Review of Smart Sensing Technologies for Monitoring Food Quality. *ACS Sens.* **2019**, *4*, 808−821.

(18) Mills, A. Oxygen Indicators and Intelligent Inks for Packaging Food. *Chem. Soc. Rev.* **2005**, *34*, 1003−1011.

(19) Brega, V.; Thomas, S. W. Red-Emitting, Acene-Doped Conjugated Polymer Nanoparticles that Respond Ratiometrically to Photogenerated $^1O_2$. *ACS Appl. Mater. Interfaces* **2021**, *13*, 13658−13665.

(20) Wang, C.-H.; Nesterov, E. E. Amplifying Fluorescent Conjugated Polymer Sensor for Singlet Oxygen Detection. *Chem. Commun.* **2019**, *55*, 8955−8958.

(21) McQuade, D. T.; Pullen, A. E.; Swager, T. M. Conjugated Polymer-Based Chemical Sensors. *Chem. Rev.* **2000**, *100*, 2537−2574.

(22) Brega, V.; Yan, Y.; Thomas, S. W. Acenes Beyond Organic Electronics: Sensing of Singlet Oxygen and Stimuli-Responsive Materials. *Org. Biomol. Chem.* **2020**, *18*, 9191−9209.

(23) Bedi, A.; Manor Armon, A.; Gidron, O. Effect of Twisting on the Capture and Release of Singlet Oxygen by Tethered Twisted Acenes. *Org. Lett.* **2020**, *22*, 7809−7813.

(24) Dong, S.; Ong, A.; Chi, C. Photochemistry of Various Acene based Molecules. *J. Photochem. Photobiol., C* **2019**, *38*, 27−46.

(25) Yang, W.; Monteiro, J. H. S. K.; de Bettencourt-Dias, A.; Catalano, V. J.; Chalifoux, W. A. Synthesis, Structure, Photophysical Properties, and Photostability of Benzodipyrenes. *Chem.—Eur. J.* **2019**, *25*, 1441−1445.

(26) You, Y. Chemical Tools for the Generation and Detection of Singlet Oxygen. *Org. Biomol. Chem.* **2018**, *16*, 4044−4060.

(27) Dorel, R.; Echavarren, A. M. Strategies for the Synthesis of Higher Acenes. *Eur. J. Org. Chem.* **2017**, *2017*, 14−24.

(28) Fudickar, W.; Linker, T. Synthesis of Pyridylanthracenes and Their Reversible Reaction with Singlet Oxygen to Endoperoxides. *J. Org. Chem.* **2017**, *82*, 9258−9262.

(29) Thorley, K. J.; Anthony, J. E. The Electronic Nature and Reactivity of the Larger Acenes. *Isr. J. Chem.* **2014**, *54*, 642−649.

(30) Zade, S. S.; Bendikov, M. Reactivity of Acenes: Mechanisms and Dependence on Acene Length. *J. Phys. Org. Chem.* **2012**, *25*, 452−461.

(31) Aubry, J.-M.; Pierlot, C.; Rigaudy, J.; Schmidt, R. Reversible Binding of Oxygen to Aromatic Compounds. *Acc. Chem. Res.* **2003**, *36*, 668−675.

(32) Altınok, E.; Smith, Z. C.; Thomas, S. W. Two-Dimensional, Acene-Containing Conjugated Polymers That Show Ratiometric

Fluorescent Response to Singlet Oxygen. *Macromolecules* **2015**, *48*, 150924092658007.
(33) Chen, X.; Tian, X.; Shin, I.; Yoon, J. Fluorescent and Luminescent Probes for Detection of Reactive Oxygen and Nitrogen Species. *Chem. Soc. Rev.* **2011**, *40*, 4783−4804.
(34) Song, B.; Wang, G.; Yuan, J. A New Europium Chelate-based Phosphorescence Probe Specific for Singlet Oxygen. *Chem. Commun.* **2005**, 3553−3555.
(35) Fudickar, W.; Linker, T. Release of Singlet Oxygen from Organic Peroxides under Mild Conditions. *ChemPhotoChem* **2018**, *2*, 548−558.
(36) Fudickar, W.; Linker, T. Reversible Photooxygenation of Alkynylanthracenes: Chemical Generation of Singlet Oxygen under Very Mild Conditions. *Chem.—Eur. J.* **2011**, *17*, 13661−13664.
(37) Pierlot, C.; Aubry, J.-M.; Briviba, K.; Sies, H.; Mascio, P. D. [1] Naphthalene Endoperoxides as Generators of Singlet Oxygen in Biological Media. *Methods Enzymol.* **2000**, *319*, 3−20.
(38) He, Y.-Q.; Fudickar, W.; Tang, J.-H.; Wang, H.; Li, X.; Han, J.; Wang, Z.; Liu, M.; Zhong, Y.-W.; Linker, T.; Stang, P. J. Capture and Release of Singlet Oxygen in Coordination-Driven Self-Assembled Organoplatinum(II) Metallacycles. *J. Am. Chem. Soc.* **2020**, *142*, 2601−2608.
(39) Filatov, M. A.; Senge, M. O. Molecular Devices based on Reversible Singlet Oxygen Binding in Optical and Photomedical Applications. *Mol. Syst. Des. Eng.* **2016**, *1*, 258−272.
(40) Zehm, D.; Fudickar, W.; Hans, M.; Schilde, U.; Kelling, A.; Linker, T. 9,10-Diarylanthracenes as Molecular Switches: Syntheses, Properties, Isomerisations and Their Reactions with Singlet Oxygen. *Chem.—Eur. J.* **2008**, *14*, 11429−11441.
(41) Zehm, D.; Fudickar, W.; Linker, T. Molecular Switches Flipped by Oxygen. *Angew. Chem., Int. Ed.* **2007**, *46*, 7689−7692.
(42) Fudickar, W.; Fery, A.; Linker, T. Reversible Light and Air-Driven Lithography by Singlet Oxygen. *J. Am. Chem. Soc.* **2005**, *127*, 9386−9387.
(43) Koylu, D.; Sarrafpour, S.; Zhang, J.; Ramjattan, S.; Panzer, M. J.; Thomas III, S. W. Acene-Doped Polymer Films: Singlet Oxygen Dosimetry and Protein Sensing. *Chem. Commun.* **2012**, *48*, 9489−9491.
(44) Yan, Y.; Lamport, Z. A.; Kymissis, I.; Thomas, S. W. Resistance to Unwanted Photo-Oxidation of Multi-Acene Molecules. *J. Org. Chem.* **2020**, *85*, 12731−12739.
(45) Zhang, J.; Smith, Z. C.; Thomas, S. W. Electronic Effects of Ring Fusion and Alkyne Substitution on Acene Properties and Reactivity. *J. Org. Chem.* **2014**, *79*, 10081−10093.
(46) Liu, K.; Lalancette, R. A.; Jäkle, F. Tuning the Structure and Electronic Properties of B-N Fused Dipyridylanthracene and Implications on the Self-Sensitized Reactivity with Singlet Oxygen. *J. Am. Chem. Soc.* **2019**, *141*, 7453−7462.
(47) Liu, K.; Lalancette, R. A.; Jäkle, F. B-N Lewis Pair Functionalization of Anthracene: Structural Dynamics, Optoelectronic Properties, and O_2 Sensitization. *J. Am. Chem. Soc.* **2017**, *139*, 18170−18173.
(48) Cobo, S.; Lafolet, F.; Saint-Aman, E.; Philouze, C.; Bucher, C.; Silvi, S.; Credi, A.; Royal, G. Reactivity of a Pyridinium-Substituted Dimethyldihydropyrene Switch under Aerobic Conditions: Self-Sensitized Photo-Oxygenation and Thermal Release of Singlet Oxygen. *Chem. Commun.* **2015**, *51*, 13886−13889.
(49) Schweitzer, C.; Schmidt, R. Physical Mechanisms of Generation and Deactivation of Singlet Oxygen. *Chem. Rev.* **2003**, *103*, 1685−1758.
(50) DeRosa, M.; Crutchley, R. J. Photosensitized Singlet Oxygen and its Applications. *Coord. Chem. Rev.* **2002**, *233*−*234*, 351−371.
(51) Kochevar, I. E.; Redmond, R. W. [2] Photosensitized Production of Singlet Oxygen. *Methods Enzymol.* **2000**, *319*, 20−28.
(52) Imran, M.; Wehrmann, C. M.; Chen, M. S. Open-Shell Effects on Optoelectronic Properties: Antiambipolar Charge Transport and Anti-Kasha Doublet Emission from a N-Substituted Bisphenalenyl. *J. Am. Chem. Soc.* **2020**, *142*, 38−43.
(53) Wehrmann, C. M.; Imran, M.; Pointer, C.; Fredin, L. A.; Young, E. R.; Chen, M. S. Spin Multiplicity Effects in Doublet versus Singlet Emission: the Photophysical Consequences of a Single Electron. *Chem. Sci.* **2020**, *11*, 10212−10219.
(54) Flors, C.; Nonell, S. On the Phosphorescence of 1H-Phenalen-1-one. *Helv. Chim. Acta* **2001**, *84*, 2533−2539.
(55) Potocny, A. M.; Teesdale, J. J.; Marangoz, A.; Yap, G. P. A.; Rosenthal, J. Spectroscopic and $^1O_2$ Sensitization Characteristics of a Series of Isomeric Re(bpy)$(CO)_3$Cl Complexes Bearing Pendant BODIPY Chromophores. *Inorg. Chem.* **2019**, *58*, 5042−5050.
(56) Li, W.; Li, L.; Xiao, H.; Qi, R.; Huang, Y.; Xie, Z.; Jing, X.; Zhang, H. Iodo-BODIPY: a Visible-Light-Driven, Highly Efficient and Photostable Metal-Free Organic Photocatalyst. *RSC Adv.* **2013**, *3*, 13417−13421.
(57) Liu, Y.; Hammitt, R.; Lutterman, D. A.; Joyce, L. E.; Thummel, R. P.; Turro, C. Ru(II) Complexes of New Tridentate Ligands: Unexpected High Yield of Sensitized $^1O_2$. *Inorg. Chem.* **2009**, *48*, 375−385.
(58) Fudickar, W.; Linker, T. Why Triple Bonds Protect Acenes from Oxidation and Decomposition. *J. Am. Chem. Soc.* **2012**, *134*, 15071−15082.
(59) Fudickar, W.; Linker, T. Theoretical Insights into the Effect of Solvents on the [4 + 2] Cycloaddition of Singlet Oxygen to Substituted Anthracenes: A Change from a Stepwise Process to a Concerted Process. *J. Phys. Org. Chem.* **2019**, *32*, No. e3951.
(60) Fudickar, W.; Linker, T. Remote Substituent Effects on the Photooxygenation of 9,10-Diarylanthracenes: Strong Evidence for Polar Intermediates. *Chem. Commun.* **2008**, 1771−1773.
(61) Turro, N. J.; Chow, M. F.; Rigaudy, J. Mechanism of Thermolysis of Endoperoxides of Aromatic Compounds. Activation Parameters, Magnetic Field, and Magnetic Isotope Effects. *J. Am. Chem. Soc.* **1981**, *103*, 7218−7224.
(62) Turro, N. J.; Chow, M.-F.; Rigaudy, J. Thermolysis of Anthracene Endoperoxides. Concerted vs. Diradical Mechanisms. Microscopic Reversibility in Endothermic Chemiluminescent Reactions. *J. Am. Chem. Soc.* **1979**, *101*, 1300−1302.

https://doi.org/10.1021/acsami.1c16033
ACS Appl. Mater. Interfaces 2022, 14, 1817−1825